Electrochemical quinuclidine-mediated C-H activation : intermediates and mechanism

Electrochemical quinuclidine-mediated C-H activation: intermediates and mechanism

Keywords: electrochemical C-H activation, analytical electrochemistry, ORR, hydrogen peroxide, quinuclidine *N*-oxide, RVC corrosion

Filip Vorobjov[1], Gilles De Smet[2], Nick Daems[1], H.Y. Vincent Ching[2], Pieter Leveque[1], Bert U. W. Maes[2], Tom Breugelmans[1*]

[1] *Research Group Applied Electrochemistry & Catalysis (ELCAT), Department of Applied Engineering, University of Antwerp, Universiteitsplein 1, 2610 Wilrijk, Belgium*
[2] *Organic Synthesis Division (ORSY), Department of Chemistry, University of Antwerp, Groenenborgerlaan 171, 2020 Antwerp, Belgium*

Abstract

The reaction mechanism of quinuclidine mediated C-H oxidation of unactivated C-H bonds has been elucidated. In-situ cathodically generated H_2O_2 was shown to diffuse to the anode where it is oxidized and participates in the ketonization reaction. Further oxidation of H_2O_2 to H_2O, O_2 and H^+ leads to glassy carbon surface degradation. Oxidation of quinuclidine was shown be kinetic-diffusion control limited and shown to be irreversible at 0 and 1 M 1,1,1,3,3,3-hexafluoroisopropan-2-ol solutions, and quasi-reversible at 0.1 M. Competing side reactions of quinuclidine with hexafluroisopropanol and hydrogen peroxide were identified that lead to decreased reaction efficiency, which explains why quinuclidine needs to be used stoichiometrically.

1 Introduction

C-H bonds are ubiquitous in organic molecules. From a synthesis perspective, the ability to functionalize inert C-H bonds offers much broader possibilities than conventional functional group transformations, as for the latter there is a need to have a pre-existing functionality in the molecule acting as a leaving group. Over the past decades the topic of C-H bond activation gained significant attention, and a plethora of synthetic protocols have been developed [1].

Among C-H bonds, the C(sp^3)-H are more demanding to functionalize compared to C(sp^2)-H bonds due to the large kinetic barrier associated with the apolar nature of the bond and lack of a π-orbital that could interact with transition metals [2] [3][4].C(sp^3)-H next to functional groups are the easiest to activate while remote functionalization is more difficult to achieve. Functional groups present in the substrate acting as"internal ligands" can bring a metal in proximity to a specific remote C-H bond allowing its activation through metallacycle formation. These coordinating moieties can be pre-installed starting from functional groups present in the substrate (directing groups[5], transient direct groups[6][7]) or by exploiting the functional groups themselves [8]. Supramolecular interactions bringing specific C-H bonds in proximity of the active center of the catalyst can also be exploited. Non-directed functionalizations, only relying on innate reactivity and the characteristics of the reagent and/or the catalyst employed, are much more challenging and face chemo- and regioselectivity issues.

Carbon oxygen bond formation is one type of C-H functionalization. Catalytic oxidation of C(sp^3)-H bonds employing oxygen as stoichiometric oxidant is a particularly attractive way to construct carbon oxygen bonds. After all, it is the most abundant and sustainable oxidant available on earth. A variety of catalysts have been employed, i.e. organocatalysts, transition metal based catalysts, photoredox catalysts, and biocatalysts.[9] One such organocatalyst is quinuclidine (Qn), first reported by MacMillan *et al.* which was activated by a transition metal based photocatalyst ($Ir[dF(CF_3)ppy]_2(dtbbpy)PF_6$).[10] The unique properties of Qn arise from its rigid structure, disfavoring internal α-C-H activation due to poor overlap of the N-C-H orbitals. Qn shows a unique selectivity for stronger, electron rich C(sp^3)-H bonds, whilst being unreactive to weaker electron poor or unsaturated C-H bonds, as well as a wide range of heteroatomic functionalities. [11] DFT calculations showed that employing a hydrogen bonding co-catalyst (tetrabutylammonium phosphate) decreased the bond dissociation energy (BDE) of the α-C-H bond in alcohols by 3 kcal mol^{-1}, which resulted in a 9-fold reaction rate enhancement.

Following the initial report of MacMillan, the majority of Qn C-H activation protocols developed employ a type of bond weakening co-catalyst such as ammonium phosphate[12], Lewis acid[13], silane[14], as well as boronic [15] and borinic [16] acids. Moreover, triple catalytic cross-coupling of C-H bonds using Qn as a hydrogen atom transfer (HAT) catalyst has been reported.[17][18][19] MacMillan *et al.*[18] reported on the direct C-H arylation of aldehydes merging photoredox, nickel and HAT catalysis where they showed that selectivity was directed by the dielectric constant of the solvent. Interestingly, structural modifications of Qn in the *C3* position was found to influence C-H activation rate.[14][19][20] Qn exhibits unprecedented selectivity based on C-H bond polarity, and enables late-stage functionalization with remarkable functional group tolerance.[20][11] Moreover, promising results in challenging carbohydrate activation are reported.[21][16][22]

In 2017 C(sp^3)-H cleavage relying on electrochemical activation of the Qn mediator has been reported by Baran *et al.* [23][24]. Interestingly, the method allows for oxidation of distal C(sp^3)-H bonds, a transformation not yet achieved in a photocatalytic setting. Moreover, reusability of the electrodes and use of atmospheric oxygen as terminal oxidant contribute to a cost-effective oxidation method. Baran's methods scalability and robustness were exemplified by a 50 g scale oxidation of sclareolide, with selectivity and yield being comparable to that of mg scale oxidation. Unfortunately Qn could not be used catalytically.

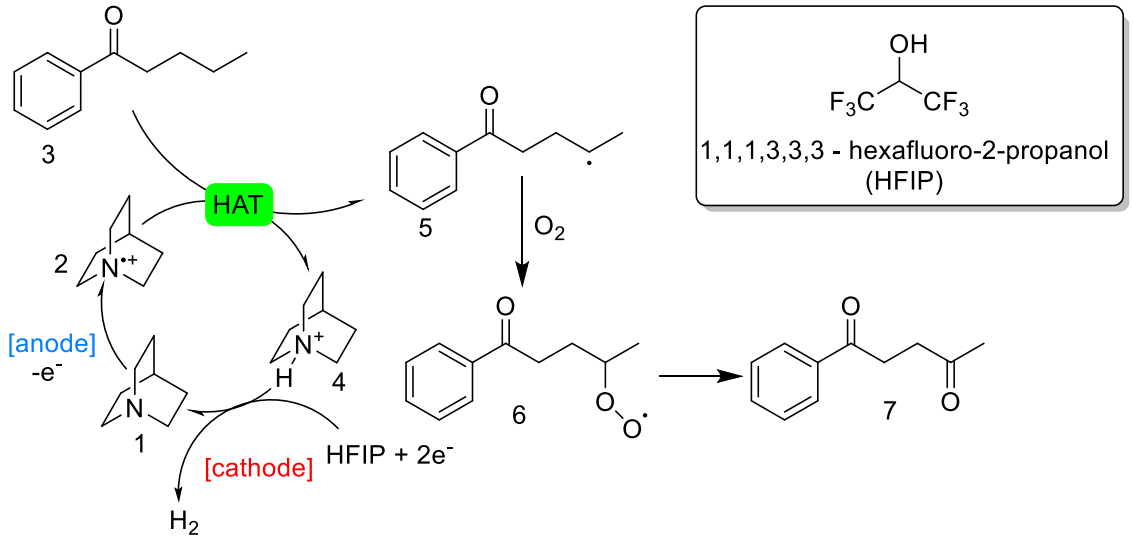

Scheme 1

Putative reaction mechanism exemplified for valerophenone (3) as proposed by Baran *et al.*[23]

Although the protocol showed broad scope and good functional group tolerance, the reaction mechanism has not been studied . The putative catalytic cycle described is presented in Scheme 1 for valerophenone (**3**). First,Qn (**1**) oxidation to $Qn^{\bullet+}$ (**2**) occurs at the anode. The formed radical cation then abstracts a hydrogen atom from a substrate (*e.g.* valerophenone **3**) via a HAT process, generating HQn^{+} (**4**) and an alkyl radical **5**. The highly reactive radical then reacts with molecular oxygen to generate a transient peroxide radical species **6**, which then via cascade reactions gets transformed to a diketone **7** (1-phenylpentane-1,4-dione). At the cathode side HQn^{+} (**4**), with the help of HFIP, generates hydrogen gas and regenerates Qn (**1**).

It can be seen 1,1,1,3,3,3-hexafluoro-2-propanol (HFIP), which is a halogenated solvent, is employed in this protocol. It is an acidic alcohol (pKa=9.3), with a high dielectric constant (ε=15.7) and low nucleophilicity, which has found many uses both in electrosynthesis[25] and C-H activation[26]. Its most notable property is the ability to stabilize cation radicals[27][28][29], which is why it is assumed that it was chosen as a co-solvent for this protocol. Baran *et al*. has attempted to use other co-solvents (TFA, and AcOH), however product yields were greatly diminished compared to that of HFIP.

In this work the mechanism of this electrochemical C(sp^3)-H oxidation protocol is elucidated, considering such data are absent in the literature. Qn oxidation at the anode, as well as oxygen reduction reaction (ORR) in the presence of HFIP at the cathode are studied. Insights into the rate limiting step and (heterogeneous) charge transfer coefficient are investigated using cyclic voltammetry. Moreover, the elusive role of HFIP, used in many C-H activation protocols [26], is unraveled here.

2 Model Reaction

Ketonization of valerophenone (**3**) into 1-phenylpentane-1,4-dione (**7**) was chosen as model reaction (Scheme 2). **3** serves as an interesting model substrate considering 1) it provides a single C-H oxidation product under the presented reaction conditions, 2) it is non-volatile, and 3) it is UV-active facilitating quantification by LC-MS and isolation using flash chromatography.

Due to its extreme electrophilicity quinuclidine cation radical abstracts the most electron rich C-H bond. The phenone moiety is electron withdrawing, decreasing proximal C-H bond electron density. As alkyl groups are considered to be weakly electron donating, the terminal methyl group is left unscathed due to having one less alkyl electron-donating group. This makes the most distal methylene group the most electron rich one, leading to its activation by quinuclidine. More detailed explanation of C-H bond reactivity can be found elsewhere[30]

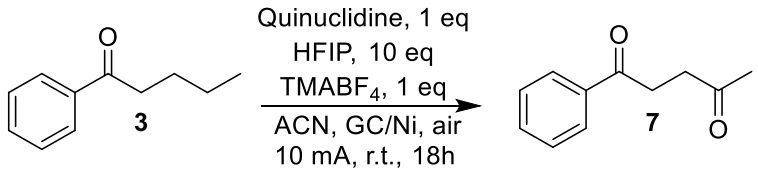

Scheme 2

Aerobic quinuclidine mediated γ-C oxidation of valerophenone (**3**) into 1-phenylpentane-1,4-dione (**7**)

The reaction was performed with 10 equivalents of HFIP with tetramethyl ammonium tetrafluoroborate ($TMABF_4$) as supporting electrolyte in acetonitrile (ACN). No considerations were made to exclude air or moisture. A vitreous carbon (RVC) anode and a nickel foam cathode were used. Stoichiometric amount of Qn was used as a mediator. A 58% yield of **7** was obtained with 35% unconverted **3** remaining. Reproduction of this reaction under the aforementioned conditions provided a similar result which was the starting point of this research.

2.1 Materials

Materials were purchased and used without further purification. Tetramethylammonium tetrafluoroborate ($TMABF_4$) (TCI, >98%) was used as electrolyte, quinuclidine (TCI, >96%) as the mediator, valerophenone (TCI, >98%) as the model substrate, acetonitrile (ACN) (Chemlab, HPLC grade >99.9%) as the solvent, and HFIP (Fluorochem, 99%) as additive. Nitrogen (Air liquide, 5N) was used to purge oxygen from the solution.

Measurements were carried out on an Autolab potentiostat (PGSTAT, AUT8251). Glassy Carbon working electrode (0.2 cm^2, Metrohm) was used as well as a Platinum Wire counter electrode (Sigma-Aldrich, 99.9%, 2.0 mm) and a non-aqueous reference electrode (ALS Co , RE-7, $Ag/AgNO_3$).

2.2 Methods

Unless otherwise specified, all procedures were carried out in an unstirred solution using a single compartment 3 electrode configuration, and potentials are given vs $Ag/AgNO_3$. Scan rate used was 100 mV s^{-1} unless stated otherwise. The working solutions comprised of 100 mM $TMABF_4$ and 10 mM quinuclidine with 100 mM of HFIP (200 µL) in ACN (19.8 mL) comprising a total volume of 20 mL, and in an inert atmosphere, unless stated otherwise.

For determination of parameters such as the charge transfer coefficient, control region, heterogeneous charge transfer coefficient a series of cyclic voltammograms with increasing scan rates were performed. The selected scan speeds were: 0.05, 0.075, 0.1, 0.125, 0.15, 0.175, 0.2, 0.3, 0.4, 0.5, 0.6, 0.7, 0.8, 0.9 and 1 V s^{-1}.

Synthesis experiments were carried out with 0.4 mmol Qn (44 mg), $TMABF_4$ (64.4 mg) and **3** (64 mg), 4 mmol HFIP (400 µL) in 3.6 mL of ACN. No considerations were given to exclude air or moisture.

For chronoamperometric (CA) and chronopotentiometric (CP) experiments a sampling rate of 0.01 s was used as well as a sampling window of 10 s in order to minimize the influence of convectional mass transport.

Electrochemical Impedance Spectroscopy (EIS) was carried out at a frequency range from 10000 to 1 Hz with a 10 mV root mean square (RMS) and 5 points were taken per decade. Data was analyzed via EIS Spectrum Analyzer (abc.chemistry.bsu.by).

As some experiments required an inert atmosphere, a sparging tube with a quick connector was placed into the reaction vessel. In order to minimize fluid losses to evaporation, a 2 stage bubbling system was used to saturate the inflowing gas with ACN vapor. During the atmosphere change, gas was vigorously bubbled though the solution for 2 minutes, after which the tube was retracted from the liquid and a slow flowrate of gas was maintained in order to have a slight overpressure in the vessel.

3 Results and discussion

3.1 E_p^{ox} and E_p^{red} peak analysis

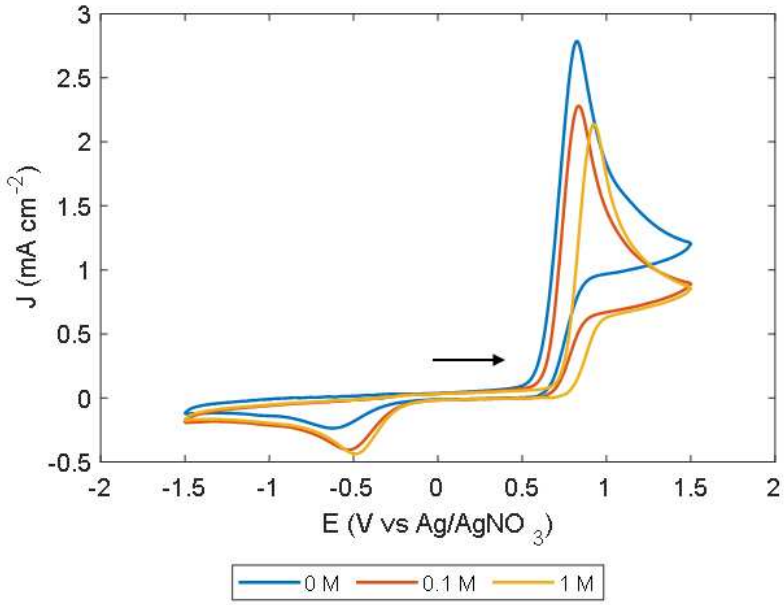

Figure 1

Cyclic Voltammetry of quinuclidine at 0, 0.1 and 1 M of HFIP. Parameters used are described in section 2.2. Black arrow indicating beginning and direction of scan.

In order to gain a better understanding of the process of Qn mediated C-H activation, a series of cyclic voltammetry (CV) experiments were carried out with varying HFIP concentration (0, 0.1 and 1 M) (fig. 1) In the forward scan direction Qn oxidation can be observed at ≈ 0.8 V. The Qn oxidation wave is irreversible on the CV timescale, which is consistent with the $Qn^{\bullet+}$ radical cation being short living[31], which is the rate limiting step of this reaction. The radical cation rapidly abstracts a hydrogen from a hydrogen source (HA), to give the HQn^+ cation. This can be expressed as a two-step process:

$$Qn \rightarrow Qn^{\cdot+} + e^- \qquad \text{(slow)} \quad \text{Eq 1}$$

$$Qn^{\cdot+} + HA \rightarrow HQn^+ + A^{\cdot} \qquad \text{(fast)} \quad \text{Eq 2}$$

Note that in general HA refers to a substrate undergoing C-H functionalization, but in its absence it can be the solvent, HFIP or the supporting electrolyte. In the presence of HFIP, the current density of the oxidation wave decreases slightly, while the peak potential becomes more positive. This effect is more pronounced at high [HFIP]. HFIP and Qn are known to form a very strong hydrogen bond (donor) (ΔH^b = -31 kJ mol^{-1})[32] which leads to a higher activation barrier and thus decreased oxidation rate. The effect is further pronounced at 1M HFIP which manifests in having a higher oxidation potential (+95 mV). This can be attributed to an even more strong hydrogen bond formation due to HFIP forming aggregates in solution at high concentrations[33][34].

On the reverse scan an irreversible reduction wave is observed at ≈ -0.6 V, corresponding to the reduction of HQn^+. It can also be seen, that with increasing concentration of HFIP the current density of the reduction peak significantly increases while the reduction potential is shifted to the positive direction. The rationale for this is that the cation is electrophilic in nature, and through hydrogen bonding with HFIP (acceptor) the electrophilicity of the cation will increase.[35]

3.2 EIS

To confirm that quinuclidine oxidation is a simple 1 step charge transfer process (eq. 1) EIS was carried out. EIS has proven to be a powerful tool which allows determination of electrical properties of materials and their interfaces, non-destructive in nature and highly sensitive. In this work we have performed EIS in the mixed kinetic/diffusion region of quinuclidine oxidation peak, (0.75 to 0.85 V depending on [HFIP]). To test the hypothesis we have decided to fit the experimental data with a standard Randles equivalent circuit with Warburg diffusion (EC) model, which can be observed in scheme 3.

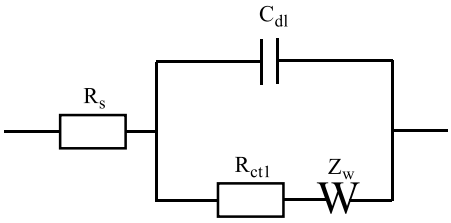

Scheme 3

Randles circuit with Warburg diffusion

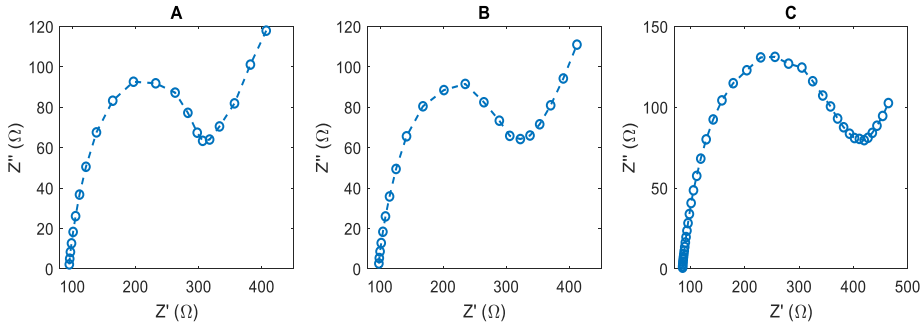

Figure 2

EIS carried out with A) 0 M HFIP at 0.75 V B) 0.1 M HFIP at 0.8 V C) 1 M HFIP at 0.85 V.

For a simple charge transfer process an EIS spectrum would include a semicircle part in the high frequency section corresponding to a charge transfer process and a linear section in the low frequency region corresponding to a diffusion process (Warburg). Fitting the experimental data, which is seen in fig. 2 into the Randles circuit from scheme 3 showed that for all [HFIP] analyzed, the n≥ 0.85 (table 1), signifying that the model indeed fits the experimental data, and quinuclidine oxidation is a simple charge transfer process. Additionally, it can be seen that at 1 M HFIP the solution is less conductive then at 0 and 0.1 M. This is explained by the fact that HFIP can solvate anions[36]. At 1 M HFIP this solvation effect becomes more pronounced, thus decreasing the solution conductivity.

	[HFIP]		
	0 M	0.1 M	1 M
R_s	95	97	85
n	0.88	0.85	0.88

Table 1
EIS simulation values for 0, 0.1 and 1M [HFIP]

3.3 Quantitative evaluation of quinuclidine oxidation

In order to gain a better understanding of quinuclidine oxidation, the reaction was evaluated on parameters such as reaction order, control region, charge transfer, diffusion and heterogeneous charge transfer coefficients.

From Eq. 1 and 2, the overall current response of the reaction can be described by:

$$I = [Qn][HA] \qquad \text{Eq 3}$$

However, due to the absence of a reversible reduction wave it can be assumed that the hydrogen atom abstraction step (Eq. 2) is fast, and in the absence of substrate the overall process will only depend on charge transfer to Qn. Thus, the reaction can be simplified to:

$$I = [Qn] \qquad \text{Eq 4}$$

This relationship then can then be used to confirm the order of the reaction.

3.3.1 Reaction order and control region

By knowing the reaction order, a better understanding of reaction kinetics in relation to reactant concentration can be achieved. Baran *et al.* utilized high reactant concentrations (0.1 M for Qn and **3**, 1 M for HFIP) to achieve good product conversion in 18h.

To confirm the reaction order, comparison between the amount of charge transferred (Q) and [QN] of 1, 2, 5, 10, and 20 mM were carried out.

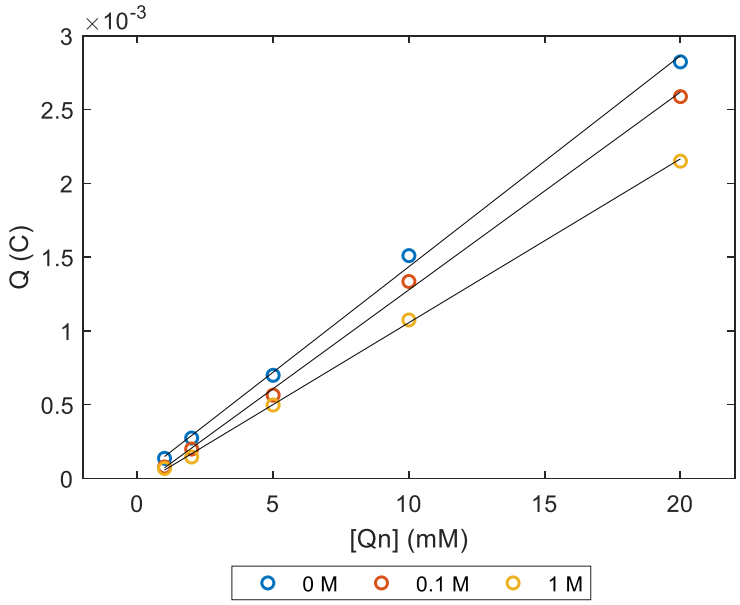

Figure 3

Plots of quinuclidine Q vs [QN]. *Data extracted from CV experiments carried out using conditions described in section 2.2*

From fig. 3 it possible to see that the reaction is 1st order in all concentrations of HFIP (R^2 = 0.9983, R^2 = 0.9986, R^2 = 0.9996 at 0, 0.1 and 1 M HFIP respectively).

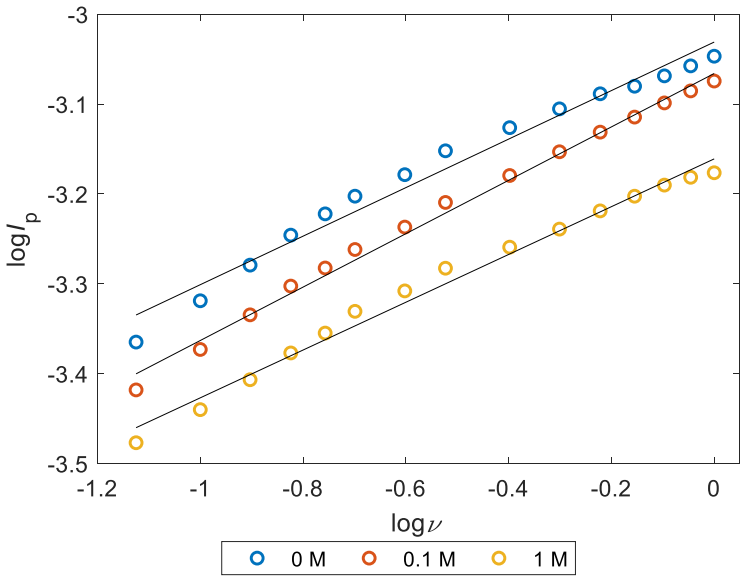

Figure 4

Plot of logI_p vs logv and linear fit lines derived from CV data. Procedure for obtaining the CV data is described in section 2.2.

To determine the bottleneck of Qn oxidation, logI_p vs log$v$ (log of peak current vs scan rate) for each HFIP concentration were plotted (fig. 4). The slope values (m) were found to be 0.2536, R^2= 0.9775, 0.3158, R^2= 0.9973, and 0.2871, R^2= 0.9877 for 0, 0.1 and 1 M HFIP, respectively. Small deviations from linearity can be observed in the plot which is due to manual data processing, however an $R^2 >$ 0.980 is sufficiently high enough to be considered a good linear fit. It can be seen that at 0.1 M HFIP m is higher than at other concentrations, suggesting that it is more diffusion controlled, meaning less kinetic limitation. However all of these values lie in between 0 (pure kinetic control) and 0.5 (pure diffusion control), suggesting that Qn oxidation is in mixed diffusion-kinetic control region.

3.3.2 Charge transfer coefficient

The charge transfer coefficient, or simply α, is a parameter used to describe kinetics of electrochemical reactions. It signifies the fraction of the interfacial potential at the electrode that helps in lowering the free energy barrier for an electrochemical reaction. It can be used to distinguish between a concerted ($\alpha < 0.5$) or stepwise mechanism ($\alpha > 0.5$). Two methods[37] were used to determine the charge transfer coefficient, based on E_p dependence on scan speed (eq 5) and on peak shape (eq 6).

$$\frac{\partial E_p}{\partial log v} = \frac{1.151RT}{\alpha_1 F} \qquad \text{Eq 5}$$

$$E_p - Ep_{/2} = \frac{1.857RT}{\alpha_2 F} \qquad \text{Eq 6}$$

Where E_p is the peak potential, $E_{p/2}$ is the half peak potential, v is the scan speed and R, F, T are universal gas and Faraday constants and temperature, respectively. The results of these calculations are summarized in Table 2.

Oxidation			Reduction		
0 M	0.1 M	1 M	0 M	0.1 M	1 M

α_1	0.441	0.345	0.410	0.181	0.183	0.343
α_2	0.068	0.066	0.057	0.129	0.158	0.144

Table 2

Summary of charge transfer coefficients (α), calculated using eq. 5 and 6.

From table 2 it can be seen that there is a discrepancy between the values in the 2 methodologies used for oxidation α determination. While eq. 5 is dependent on the shift of peak potential to the square root of the scan rate and is more reliable in determination of α, the eq. 6 for α_2 is derived from the peak shape. The shape of the peak can change depending on various physical phenomena, such as, for example, adsorption. Such a discrepancy in the values therefore suggests that quinuclidine oxidation involves an adsorption step prior to oxidation, with subsequent desorption of the cation radical. The reduction α values are much closer to each other at 0 M and 0.1 M HFIP, suggesting that there is no adsorption of the HQn^+ species during its reduction. Both oxidation and reduction α values suggest that the reactions proceed through a concerted pathway, which involves high energy intermediates.

3.3.3 Diffusion coefficient

The diffusion coefficient (*D*) is an important parameter in electrochemistry, as it describes the diffusional transport of the analyte to the electrode surface. It can be employed in kinetic equations, estimate surface area of an electrode, *etc*. In this work we are interested how HFIP influences the *D* value of Qn, as well as to gain insights into reaction kinetics.

For the determination of *D* we have utilized time dependent techniques (Cottrell equations (eq 7) and Sand (eq 8)). The general limitation of time dependent techniques is the duration of the experiment, since with a buildup of a gradient of concentrations at the electrode interface other mass transport effects such as convective interference may make accurate measurements difficult. Measurements in water and other fluid solvents are difficult to keep accurate longer than 300 s, and even 20 s may show some convective interference.[37]

$$I = \frac{nFAC\sqrt{D}}{\sqrt{\tau\pi}} \qquad \text{Eq 7}$$

$$\sqrt{\tau} = \frac{nFCA\sqrt{\pi D}}{2I} \qquad \text{Eq 8}$$

Where *I* is current, I_p is peak current, τ is time, *C* is concentration, *A* is the electrode area, *n* is the number of electrons transferred, ν is the scan speed and π and *F* have their usual meanings.

	D ($cm^2\ s^{-1}$)		
	0 M	0.1 M	1 M
Cottrell	$2.67x10^{-5}$	$2.00x10^{-5}$	$1.84x10^{-5}$
Sand	$1.92x10^{-5}$	$1.90x10^{-5}$	$1.17x10^{-5}$

Table 3

Summary of diffusion coefficients

A summary of *D* values can be seen in table 3. The Cottrell and Sand equations give similar values, where *D* decreases as HFIP concentration increases, which is consistent with the viscosity of HFIP being much higher than that of ACN. We have not found any information on *D* for Qn in ACN, however for structurally similar 1,4-diazabicyclo[2.2.2]octane (DABCO) , $D = 1.52 \cdot 10^{-5}\ cm^2\ s^{-1}$ [38], which closely matches the results from the Sand equation (0 M HFIP). This makes us believe that this approaches is the most suitable to determine the actual diffusion coefficient of Qn.

3.3.4 Heterogeneous Charge Transfer Coefficient

The heterogeneous charge transfer coefficient (k^0), or the *standard rate of electron transfer*, is a fundamental parameter that is used in electrochemistry to quantify the reaction rate of an electrochemical process. By knowing k^0, a better understanding of kinetics can be achieved, and effectiveness of various charge transfer mediators can be evaluated. In this paper, the charge transfer coefficient was determined by the method of Kochi[39] (eq 9).

$$k^0 = 2.18\sqrt{\frac{DnFv\alpha_1}{RT}}exp\left(-\frac{\alpha_1^2 nF(E_{p,a}-E_{p,c})}{RT}\right) \qquad \text{Eq 9}$$

As can be seen from eq 9, the Kochi method relies on the separation of E_p^{ox} and E_p^{red} , and can be used to determine k^0 of irreversible systems.

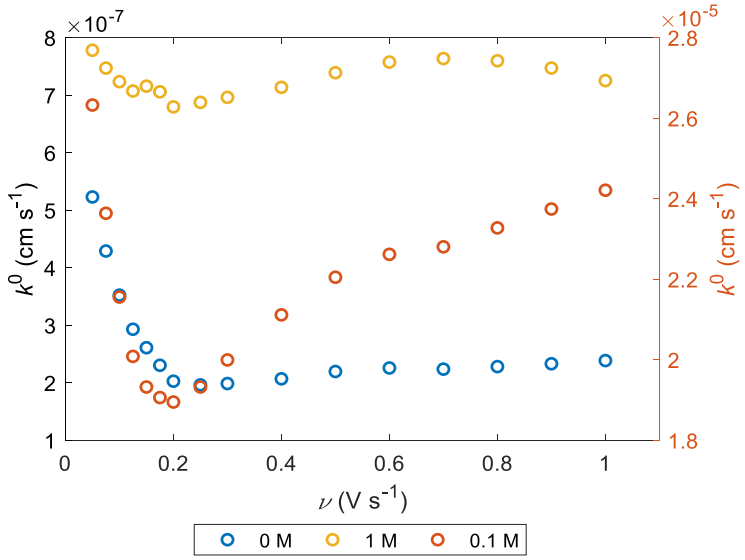

Figure 5

Heterogeneous charge transfer coefficient dependence on [HFIP]. 0.1 M y-axis is on the right.

In fig. 5 the evolution of the heterogeneous charge transfer coefficient is shown. It can be observed immediately that k^0 at 0.1 M HFIP is 2 orders of magnitude higher than 0 and 1 M. The shape of the plot arises from the combined contribution of the kinetic part at lower scan speeds up to 0.2 V s^{-1} of the Kochi-Klinger equation (2^{nd} part of the eq 9) and diffusional part (after 0.2 V s^{-1}) (1^{st} part of eq 9) at higher scan rates, confirming a mixed kinetic-diffusion controlled reaction. At 0 M it can be observed that the k^0 is highest at low scan rates, indicating a more kinetically limited reaction, whilst at 1 M the kinetic contribution is diminished in comparison with the diffusional one. From this it is possible to conclude that at 0 M HFIP quinuclidine oxidation experiences the highest kinetic limitation, whilst at 1 M it is mostly diffusion limited, albeit the rate of oxidation is much smaller than at 0.1 M. It is worth noting that in all concentrations tested there is both influence of diffusion and kinetic limitation, suggesting all of these reactions fall in the mixed diffusion-kinetic control.

3.4 Oxygen Reduction Reaction

In the absence of O_2 no products were detected by us or in the work of Baran *et al.* It was also found that when the anodic and cathodic compartments were separated by an anion exchange membrane (Xergy, DURION 20 µm) no products were detected. Therefore, we have looked into the oxygen reduction reaction (ORR) at the cathode and how it impacts the target reaction. Oxygen reduction in

non-aqueous solutions is well studied in the absence[40][41] and presence of proton sources [42]. Here, HFIP is a proton source (pKa = 9.3 in H_2O [43] and 17.9 in DMSO[44]).

In the absence of protons, the one electron reduction of O_2 leads to the superoxide radical anion ($O_2^{\bullet-}$, eq 10) which is relatively stable in aprotic solutions [45]. However, in the presence of protons the reaction becomes a 2 electron process, in which H_2O_2 is generated[46], which can be seen in eq 11.

$$O_2 + e^- \leftrightarrow O_2^{-\cdot} \qquad \text{Eq 10}$$

$$O_2 + 2e^- + 2HA \rightarrow H_2O_2 + 2A^- \qquad \text{Eq 11}$$

$$H_2O_2 + 2e^- + 2HA \rightarrow 2H_2O + 2A^- \qquad \text{Eq 12}$$

Fig. 6 shows the evolution of the ORR reaction with increasing concentration of HFIP.

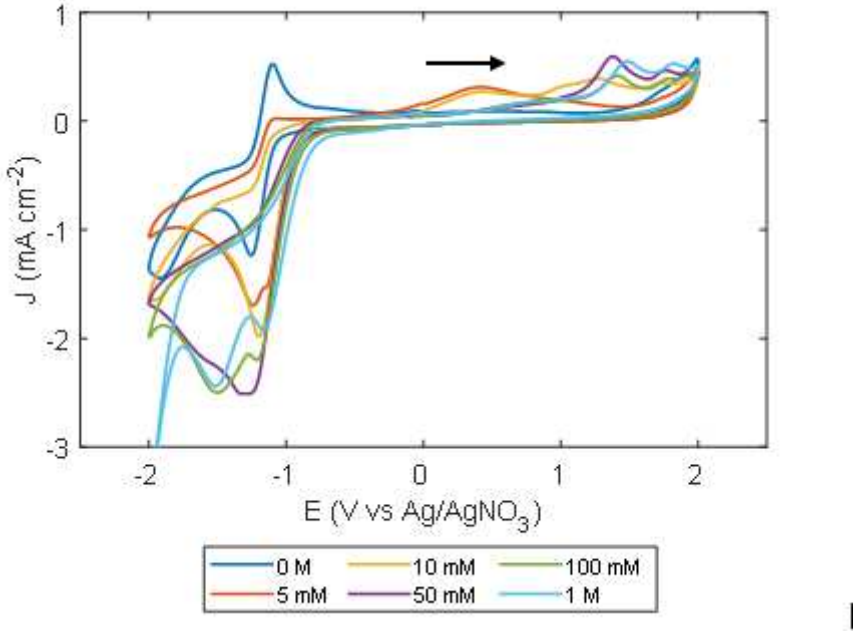

Figure 6

HFIP influence on ORR

CV of air saturated solution with HFIP gradient.
Black arrow indicating start and direction of scan

Without protons (0 M HFIP) a quasi-reversible peak at E_p= -1.25 V is observed (fig. 6) consistent with Eq 10. Addition of increasing amounts of HFIP to the solution changes the reaction from quasi-reversible to irreversible due to formation of H_2O_2, which is consistent with eq. 12. The 2nd reduction peak observed at -1.5 V is assigned to further reduction of H_2O_2 to H_2O, consistent with eq 12.

Although in the electrosynthetic procedure described by Baran *et al*. the authors used RVC_{anode} and Ni $foam_{cathode}$, for kinetic investigations we have used a GC_{anode} and Pt $wire_{cathode}$. The influence of the counter electrode material for this investigation expected to be minimal since the analytical methods used (CV etc.) ORR/OER reaction at the surface of the working (GC) electrode is studied.

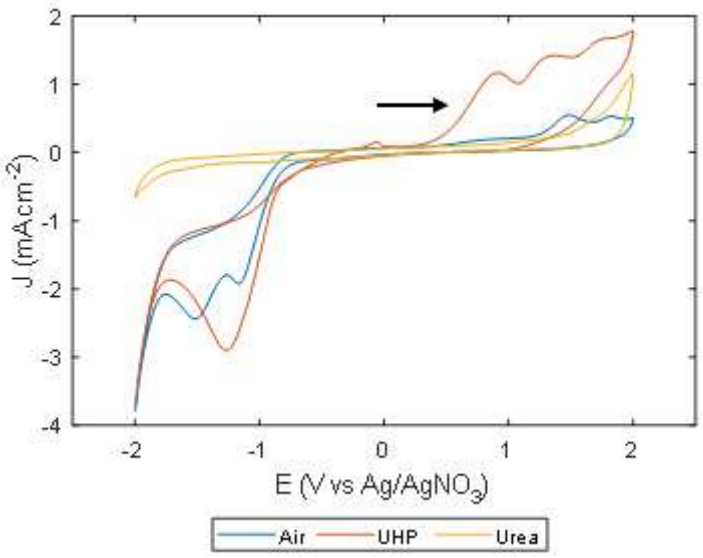

Figure 7

Cyclic Voltammetry of UHP, Urea and using standard conditions described in section 2.3. Black arrow indicating start and direction of scan

CVs (fig. 7) performed with anhydrous urea hydrogen peroxide (UHP), urea, as well as O_2 in 1 M of HFIP confirmed that the oxidation peaks can be attributed to H_2O_2. It can be seen that in the scanned potential range urea is not electrochemically active. The 1st oxidation peak that is seen at 1 V is putatively attributed to adsorption of H_2O_2 to the surface of the electrode[47], an effect that is much more pronounced in UHP due to higher [H_2O_2]. The 2nd oxidation peak is that of H_2O_2, and follows the pathway shown in eq 13-14.[48]. The 3rd peak is attributed to water oxidation, seen in eq 15. Indeed, during prolonged electrolysis of UHP bubble formation could be seen on the anode, confirming this H_2O_2 decomposition pathway.

$$H_2O_2 \rightarrow HO_2^{\cdot} + H^+ + e^- \qquad \text{Eq 13}$$

$$HO_2^{\cdot} \rightarrow \uparrow O_2 + H^+ + e^- \qquad \text{Eq 14}$$

$$2H_2O \rightarrow \uparrow O_2 + 4H^+ + 4e^- \qquad \text{Eq 15}$$

With respect to the Qn mediated C-H bond activation, H_2O_2 is stable enough to diffuse from the cathode to the anode. At the surface of the anode H_2O_2 is oxidized to give $HO_2^{\bullet}$ (eq 13) as an intermediate [48], which can participate in the C-H activation process via a radical-radical coupling mechanism. However, the relationship of HFIP and H_2O_2 is not so straight forward as it seems. Although H_2O_2 by itself is a strong oxidant, in combination with HFIP its oxidative ability is enhanced 10^5 fold (relative to 1,4-dioxane as solvent)[49]. Indeed, using density functional theory (DFT) Berkessel *et al.*[49] demonstrated that aggregates of 3 HFIP molecules binding via hydrogen bonding to other HFIP and H_2O_2 oxygen atoms in a synergistic effect yield the lowest activation barrier of oxidation H_2O_2 (Scheme 4).

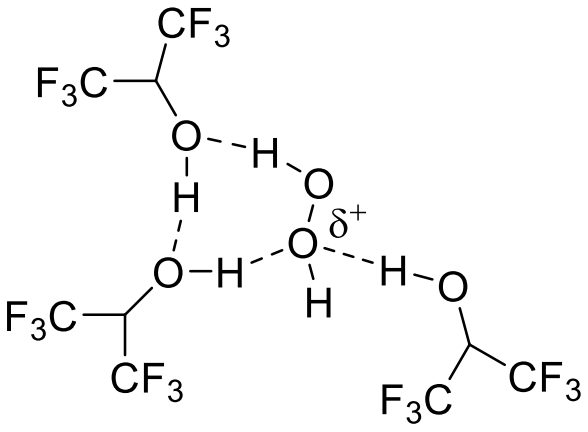

Scheme 4

Example of HFIP clustering and activation of H_2O_2

To confirm that the reaction does indeed proceed through a peroxide intermediate, a 30% solution of H_2O_2 (1.2 eq) was added to the solution and oxygen was removed by purging the solution with argon. Although water disrupts the HFIP hydrogen bonding networks, even a 1:1 ratio of HFIP/H_2O_2 still produces a catalytic effect [48], so trace amounts of the diketone product were detected (LC/MS), with many side products, presumably due to electrode surface being degraded by radicals generated through water oxidation[50]. Similarly, incorporating UHP (1.2 eq) also lead to detectable product. All of this evidence suggests that H_2O_2 is indeed the reactive intermediate in this reaction.

3.5 Concurrent processes

3.5.1 Surface Oxidation

It was observed that the reticulated vitreous carbon (RVC) foam, which was also used by Baran *et al.*, experienced a big drop in activity even after 1 chronoamperometric synthesis experiment. Also, a thin diffractive layer was formed on the surface of the electrode. To gain a better understanding of the process of surface deactivation, we have analyzed the electrode surface using ATR-FT/IR. Samples were prepared by drying and grinding the electrodes to a fine powder. Measurements were made in the frequency range from 4000 to 500 cm^{-1}.

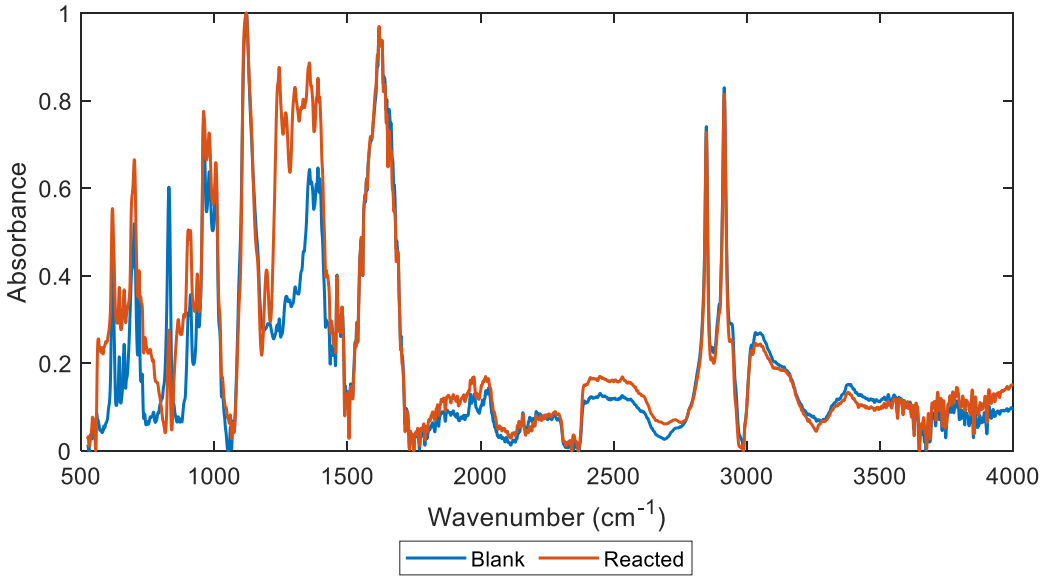

Figure 8

ATR-FT/IR spectra of unreacted surface (blue) and after reaction (red) of RVC foam . Spectra were baseline corrected and normalized to the highest peak.

From fig. 8 it is possible to see that there is a significant difference between the spectra in the region of 1200 to 1400 cm^{-1}. The peaks in this region can be assigned to various vibration modes of carbon-oxygen bonds, such as aliphatic ether C-O stretching (1195 cm^{-1}), vinyl ether C-O stretching (1242 cm^{-1}), alkyl aryl ether C-O stretching (1268 cm^{-1}) and aromatic ether C-O stretching (1298 cm^{-1}). Additionally, presence of amines on the surface can't be ruled out, as the band at 1334 cm^{-1} can be attributed to aromatic amine C-N stretching.
Corrosion of glassy carbon surfaces was studied by Yi *et al.* [50]. The authors reported that under acidic conditions and in the presence of water the surface of glassy carbon gets covered with various oxides, which bind irreversibly to the active sites of the surface. These observations fall in line with ours, therefore confirming surface deactivation through formation of oxides. A putative surface oxidation and degradation pathway can be viewed in scheme 6D.

3.5.2 Side Reactions

Surprisingly, GC-MS analysis of the reaction mixture revealed the presence of hexafluoroacetone (HFA), an oxidation product of HFIP. Running experiments in chronopotentiometric mode produced substantially more HFA than in chronoamperometric mode. Initially we speculated that the high concentration of HFA in this case might be related to direct oxidation of HFIP at the surface of the glassy carbon electrode, as the potential there rises above the HFIP oxidation potential (≈2 V). However, HFA was also detected while experiments were performed in CA, in which the potential stays below the HFIP oxidation potential. HFA is observed because HFIP only C-H bond is susceptible to HAT by $Qn^{\bullet+}$ (**4**). The hydrogen generated by -OH moieties' oxidation possibly further participates in anodic surface degradation. Initially it was assumed that the adduct of HFIP and Qn would increase the C-H bond hydricity of HFIP. However our DFT results suggested that it is the unbounded HFIP C-H bond that possesses the highest hydricity, and therefore is most likely to be activated by $Qn^{\bullet+}$. More information on DFT can be found in the SI. Having this unwanted side reaction decreases the rate of HAT from the substrate **3** to $Qn^{\bullet+}$ (**4**) thus decreasing the overall process efficiency.

3.5.3 Quinuclidine Deactivation

In principle, only catalytic amounts of Qn should be necessary for electrosynthesis, however stoichiometric amount are required to achieve good conversion. To understand the reasoning behind this, we have looked into possible quinuclidine deactivation pathways. When analyzing LC-MS chromatograms of the reacted mixtures we have found that the quinuclidine present in solution was oxidized to quinuclidine *N*-oxide. Laus [51] showed that tertiary amines can be oxidized to corresponding *N*-oxides with H_2O_2, and the presence of ACN accelerates this process. To understand if it is indeed a deactivated form of the mediator, we have synthesized quinuclidine *N*-oxide (synthesis procedure can be found in SI) and incorporated into the synthesis procedure described in section 2.2. After 18 h of electrolysis only trace desired product was formed.

From this it is possible to conclude that although H_2O_2 is essential for the ketonization of the substrate, ever increasing concentration of H_2O_2 which is continuously generated at the cathode oxidizes the mediator over time leaving less of the active form to participate in the desired C-H activation reaction.

4 Proposed catalytic cycle

Based on the information gathered from the performed experiments, a new reaction mechanism is given including all the desired and undesired ongoing reactions (Scheme 6).

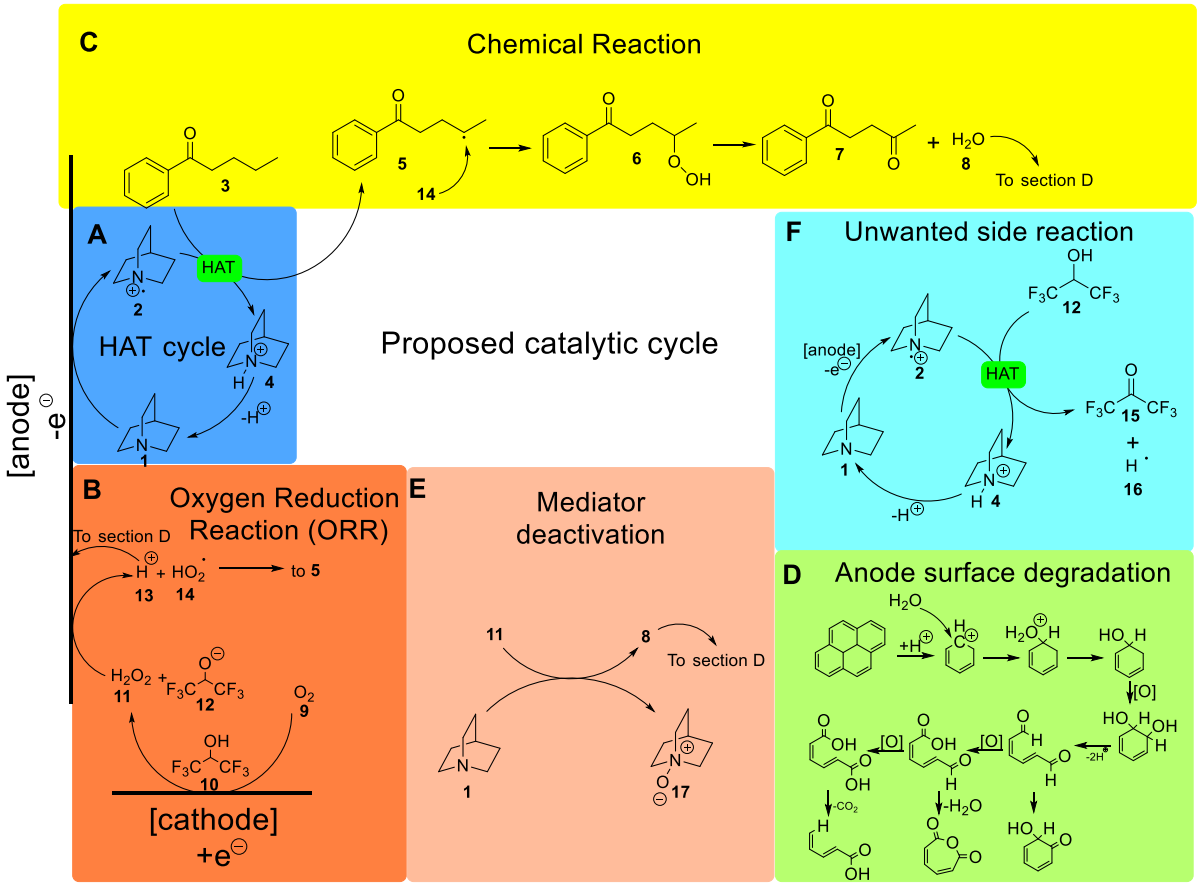

Scheme 6

Proposed catalytic cycle.

Scheme 6D is redrawn from [50] *and represents possible active site deactivation and dissolution of the GC or RVC surface. No work was done to investigate actual GC surface degradation products.*

The proposed catalytic cycle starts from mediator (**1**) oxidation at the anode to a cation radical (**2**), which then abstracts a hydrogen atom from substrate **3**, to produce an alkyl radical **5** and a cation (**4**) which is in full accordance with what was proposed initially by Baran *et al.* (Scheme 2). However, we did not find support for the regeneration of **1** from **4** at the cathode with the assistance of HFIP, concomitantly producing H_2 (Scheme 2). Instead at the cathode side oxygen (**9**) via 2 electron and 2 proton transfer from 2 HFIP molecules (**10**) is reduced to form hydrogen peroxide (**11**) and hexafluoroisopropanolate (**12**). **11** then diffuses to the anode side, where an electron is removed, which causes the peroxide to split into a proton (**13**) and a hydroperoxyl radical (**14**). Subsequently, **14** reacts with the alkyl radical **5** via a radical-radical coupling mechanism to produce valerophenone peroxide (**6**). Due to the reduction of the O-O bond and oxidation of α-CH bond in **6** water **8** is eliminated providing 1-phenylpentane-1,4-dione (**7**) product. Concurrently, HFIP (**12**) undergoes a HAT reaction with **2** and subsequent internal oxidation to produce a volatile byproduct, i.e. hexafluoroacetone (HFA) (**15**) and H• (**16**) (scheme 6, F). This process is in direct competition with the C-H activation protocol of **3** by $Qn^{\bullet+}$ (**2**) and therefore decreases the overall process efficiency. Additionally, HFIP (**10**) is consumed rationalizing the required excess. Noteworthy, protons (**13**) and water (**8**) formed in the process cause degradation of the glassy carbon electrode through further oxidation (sheme 6, D). [50] Concurrently to the mediator cycle (**1**-**2**,**4**), deactivation of the mediator Qn (**1**) occurs via oxidation by hydrogen peroxide (**11**) to yield the corresponding quinuclidine *N*-oxide (**17**) and water (**8**).

5 Conclusion

The reaction mechanism of aerobic quinuclidine mediated C(sp^3)-H oxidation of unactivated C(sp^3)-H bonds has been elucidated. The intermediates that are generated in this C-H activation process, using valerophenone (**3**) as a model substrate, were identified using conventional electrochemical techniques (i.e. cyclic voltammetry, chronoamperometry, chronopotentiometry, EIS) as well as ATR-FT/IR. It was found that the reaction is 1st order, and that Qn oxidation proceeds through a concerted pathway, and is first adsorbed to the surface of the electrode. The reduction of the quinuclidine cation also proceeds through a concerted pathway, however does not adsorb to the surface. Analysis of the heterogeneous charge transfer coefficient (k^0) indicated that the reaction is irreversible at 0 and 1 M HFIP, however quasireversible at 0.1 M HFIP, indicating that the latter concentration is favorable for the forward quinuclidine oxidation reaction. At all concentrations of HFIP the charge transfer to quinuclidine is under diffusion-kinetic control, which offers possibilities to increase the reaction rate with e.g. structurally modified quinuclidines.

It was found that ORR at the cathode side in the presence of HFIP generates H_2O_2, which then diffuses to the cathode side and participates in the reaction cycle. Strong hydrogen bonding properties as well as low nucleophilicity of HFIP enables H_2O_2 to participate in this C-H activation protocol through formation of a hydroperoxyl radical. Further oxidation of H_2O_2 and H_2O to O_2 and H^+ leads to formation of oxides at the glassy carbon surface, decreasing its activity. An unwanted side reaction of HFIP anion with $Qn^{\bullet+}$, providing an undesirable C-H activation pathway, and electron uptake at the anode producing HFA has been discovered to compete with the desired substrate C-H activation pathway, decreasing the overall efficiency. HFIP consumption in the ORR and HFA formation is therefore the justification why it needs to be used in large excess.

Finally, with increasing concentration of H_2O_2 in the solution, Qn forms an *N*-oxide which is the inactive form of the mediator, leaving less of the active form to participate in the C-H activation process, thereby explaining incomplete conversion of valerophenone. This rationalizes why Qn cannot be used catalytically.

Potential further improvements of the reaction include replacing the ORR with another reaction that does not involve H_2O_2 formation, which would also allow a lower [HFIP] to be used. Introduction of this system into a continuous flow electrolyzer can greatly improve the reaction efficiency by introducing convectional mass transport. Finally, the kinetics of the reaction could be improved by incorporating structurally modified quinuclidines into the reaction. Work to improve the reaction is currently underway is our research group.

Acknowledgements

This work was supported by University of Antwerp Special Research Fund (BOF), award number FFB180163.

Declaration of Competing Interest

The authors declare that they have no known competing financial interests or personal relationships that could have appeared to influence the work reported in this paper.

Bibliography

[1] T. Rogge *et al.*, “C–H activation,” *Nat. Rev. Methods Prim.*, vol. 1, no. 1, p. 43, Dec. 2021, doi: 10.1038/s43586-021-00041-2.

[2] Y. Q. Li, Q. L. Yang, P. Fang, T. S. Mei, and D. Zhang, “Palladium-Catalyzed C(sp^2)-H Acetoxylation via Electrochemical Oxidation,” *Org. Lett.*, vol. 19, no. 11, pp. 2905–2908, 2017, doi: 10.1021/acs.orglett.7b01138.

[3] B. Liu, A. M. Romine, C. Z. Rubel, K. M. Engle, and B. F. Shi, “Transition-Metal-Catalyzed, Coordination-Assisted Functionalization of Nonactivated C(sp^3)-H Bonds,” *Chem. Rev.*, vol. 121, no. 24, pp. 14957–15074, 2021, doi: 10.1021/acs.chemrev.1c00519.

[4] K. Murali *et al.*, “Decoding Directing Groups and Their Pivotal Role in C−H Activation,” *Chem. - A Eur. J.*, vol. 27, no. 49, pp. 12453–12508, 2021, doi: 10.1002/chem.202101004.

[5] C. Sambiagio *et al.*, “A comprehensive overview of directing groups applied in metal-catalysed C-H functionalisation chemistry,” *Chem. Soc. Rev.*, vol. 47, no. 17, pp. 6603–6743, 2018, doi: 10.1039/c8cs00201k.

[6] C. Jacob, B. U. W. Maes, and G. Evano, “Transient Directing Groups in Metal−Organic Cooperative Catalysis,” *Chem. - A Eur. J.*, vol. 27, no. 56, pp. 13899–13952, 2021, doi: 10.1002/chem.202101598.

[7] N. Goswami, T. Bhattacharya, and D. Maiti, “Transient directing ligands for selective metal-catalysed C–H activation,” *Nat. Rev. Chem.*, vol. 5, no. 9, pp. 646–659, 2021, doi: 10.1038/s41570-021-00311-3.

[8] J. Das, D. K. Mal, S. Maji, and D. Maiti, “Recent Advances in External-Directing-Group-Free C-H Functionalization of Carboxylic Acids without Decarboxylation,” *ACS Catal.*, vol. 11, no. 7, pp. 4205–4229, 2021, doi: 10.1021/acscatal.1c00176.

[9] H. Sterckx, B. Morel, and B. U. W. Maes, “Catalytic Aerobic Oxidation of C(sp^3)−H Bonds,” *Angew. Chemie - Int. Ed.*, vol. 58, no. 24, pp. 7946–7970, 2019, doi: 10.1002/anie.201804946.

[10] J. L. Jeffrey, J. A. Terrett, and D. W. C. MacMillan, “O-H hydrogen bonding promotes H-atom transfer from α-C-H bonds for C-alkylation of alcohols,” *Science (80-.).*, vol. 349, no. 6255, pp. 1532–1536, 2015, doi: 10.1126/science.aac8555.

[11] W. Xiao, X. Wang, R. Liu, and J. Wu, “Quinuclidine and its derivatives as hydrogen-atom-transfer catalysts in photoinduced reactions,” *Chinese Chem. Lett.*, vol. 32, no. 6, pp. 1847–1856, 2021, doi: 10.1016/j.cclet.2021.02.009.

[12] I. C. Wan, M. D. Witte, and A. J. Minnaard, “Site-selective carbon-carbon bond formation in unprotected monosaccharides using photoredox catalysis,” *Chem. Commun.*, vol. 53, no. 36, pp. 4926–4929, 2017, doi: 10.1039/c7cc01416c.

[13] J. Twilton, M. Christensen, D. A. DiRocco, R. T. Ruck, I. W. Davies, and D. W. C. MacMillan, “Selective Hydrogen Atom Abstraction through Induced Bond Polarization: Direct α-Arylation of Alcohols through Photoredox, HAT, and Nickel Catalysis,” *Angew. Chemie - Int. Ed.*, vol. 57, no. 19, pp. 5369–5373, 2018, doi: 10.1002/anie.201800749.

[14] K. Sakai, K. Oisaki, and M. Kanai, “Identification of Bond-Weakening Spirosilane Catalyst for Photoredox α-C–H Alkylation of Alcohols,” *Adv. Synth. Catal.*, doi: 10.1002/adsc.201901253.

[15] E. Article, G. Hughes, and M. S. Taylor, “Chemical Science using a combined arylboronic acid / photoredox catalyst system” vol. 1, pp. 1–7, 2019, doi: 10.1039/c9sc05173b.

[16] V. Dimakos, H. Y. Su, G. E. Garrett, and M. S. Taylor, “Site-Selective and Stereoselective C-H Alkylations of Carbohydrates via Combined Diarylborinic Acid and Photoredox Catalysis,” *J. Am. Chem. Soc.*, vol. 141, no. 13, pp. 5149–5153, 2019, doi: 10.1021/jacs.9b01531.

[17] C. Le, Y. Liang, R. W. Evans, X. Li, and D. W. C. MacMillan, “Selective C(sp^3)-H alkylation via polarity-match-based cross-coupling,” *Nature*, vol. 547, no. 7661, pp. 79–83, 2017, doi: 10.1038/nature22813.

[18] X. Zhang and D. W. C. MacMillan, “Direct Aldehyde C-H Arylation and Alkylation via the Combination of Nickel, Hydrogen Atom Transfer, and Photoredox Catalysis,” *J. Am. Chem.*

Soc., vol. 139, no. 33, pp. 11353–11356, 2017, doi: 10.1021/jacs.7b07078.

[19] M. H. Shaw, V. W. Shurtleff, J. A. Terrett, J. D. Cuthbertson, and D. W. C. MacMillan, "Native functionality in triple catalytic cross-coupling: C(sp^3)-H bonds as latent nucleophiles," *Science (80-.).*, vol. 352, no. 6291, pp. 1304–1308, 2016, doi: 10.1126/science.aaf6635.

[20] H. Bin Yang, A. Feceu, and D. B. C. Martin, "Catalyst-Controlled C-H Functionalization of Adamantanes Using Selective H-Atom Transfer," *ACS Catal.*, vol. 9, no. 6, pp. 5708–5715, 2019, doi: 10.1021/acscatal.9b01394.

[21] Y. Wang, H. M. Carder, and A. E. Wendlandt, "Synthesis of rare sugar isomers through site-selective epimerization," *Nature*, vol. 578, no. 7795, pp. 403–408, 2020, doi: 10.1038/s41586-020-1937-1.

[22] M. Kidonakis, A. Villotet, M. Witte, S. Beil, and A. Minnaard, "Site-selective Electrochemical Oxidation of Glucosides," *ChemRxiv*, 2022, doi: 10.26434/chemrxiv-2022-gg3g5.

[23] Y. Kawamata *et al.*, "Scalable, Electrochemical Oxidation of Unactivated C-H Bonds," *J. Am. Chem. Soc.*, vol. 139, no. 22, pp. 7448–7451, 2017, doi: 10.1021/jacs.7b03539.

[24] C. Sambiagio, H. Sterckx, and B. U. W. Maes, "Electrosynthesis: A New Frontier in Aerobic Oxidation?," *ACS Cent. Sci.*, vol. 3, no. 7, pp. 686–688, 2017, doi: 10.1021/acscentsci.7b00275.

[25] J. M. Ramos-Villaseñor, E. Rodríguez-Cárdenas, C. E. Barrera Díaz, and B. A. Frontana-Uribe, "Review—Use of 1,1,1,3,3,3–hexafluoro–2–propanol (HFIP) Co-Solvent Mixtures in Organic Electrosynthesis," *J. Electrochem. Soc.*, vol. 167, no. 15, p. 155509, 2020, doi: 10.1149/1945-7111/abb83c.

[26] S. K. Sinha, T. Bhattacharya, and D. Maiti, "Role of hexafluoroisopropanol in C-H activation," *React. Chem. Eng.*, vol. 4, no. 2, pp. 244–253, 2019, doi: 10.1039/c8re00225h.

[27] L. Eberson, M. P. Hartshorn, and O. Persson, "1,1,1,3,3,3-Hexafluoropropan-2-ol as a solvent for the generation of highly persistent radical cations," *J. Chem. Soc. Perkin Trans. 2*, no. 9, pp. 1735–1744, 1995, doi: 10.1039/p29950001735.

[28] L. Eberson, M. P. Hartshorn, O. Persson, and F. Radner, "Making radical cations live longer," *Chem. Commun.*, no. 18, pp. 2105–2112, 1996, doi: 10.1039/cc9960002105.

[29] L. Eberson, M. P. Hartshornb, and O. Perssona, "Generation of Solutions of Highly Persistent Radical Cations by 4-Tolylthallium(III) Bis)trifluoroacetate) in 1,1,1,3,3,3-hexafluoropropan-2-ol," *J. Chem. Soc. Chem. Commun.*, vol. 11, no. iii, pp. 1131–1132, 1995, doi: 10.1039/C39950001131.

[30] T. Newhouse and P. S. Baran, "If C-H bonds could talk: Selective C-H bond oxidation," *Angew. Chemie - Int. Ed.*, vol. 50, no. 15, pp. 3362–3374, 2011, doi: 10.1002/anie.201006368.

[31] T. A. Brown, H. Chen, and R. N. Zare, "Detection of the Short-Lived Radical Cation Intermediate in the Electrooxidation of N,N-Dimethylaniline by Mass Spectrometry," *Angew. Chemie - Int. Ed.*, vol. 54, no. 38, pp. 11183–11185, 2015, doi: 10.1002/anie.201506316.

[32] N. C. Maiti, Y. Zhu, I. Carmichael, A. S. Serianni, and V. E. Anderson, "$^1J_{CH}$ correlates with alcohol hydrogen bond strength," *J. Org. Chem.*, vol. 71, no. 7, pp. 2878–2880, 2006, doi: 10.1021/jo052389k.

[33] A. Berkessel and J. A. Adrio, "Kinetic studies of olefin epoxidation with hydrogen peroxide in 1,1,1,3,3,3-hexafluoro-2-propanol reveal a crucial catalytic role for solvent clusters," *Adv. Synth. Catal.*, vol. 346, no. 2–3, pp. 275–280, 2004, doi: 10.1002/adsc.200303222.

[34] A. Berkessel, J. Mars, M. Mezger, A. Wiebe, S. R. Waldvogel, and B. Kirchner, "The Catalytic Effect of Fluoroalcohol Mixtures Depends on Domain Formation," 2017, doi:

10.1021/acscatal.6b03090.

[35] E. M. D'Amato, J. Börgel, and T. Ritter, "Aromatic C-H amination in hexafluoroisopropanol," *Chem. Sci.*, vol. 10, no. 8, pp. 2424–2428, 2019, doi: 10.1039/C8SC04966A.

[36] N. Shida, Y. Imada, S. Nagahara, Y. Okada, and K. Chiba, "Interplay of arene radical cations with anions and fluorinated alcohols in hole catalysis," *Commun. Chem.*, vol. 2, no. 1, pp. 3–5, 2019, doi: 10.1038/s42004-019-0125-4.

[37] A. J. Bard and L. R. Faulkner, *Electrochemical Methods: Fundamentals and Applications*, 2nd ed. John Wiley & Sons, Incorporated, 2000, 2001.

[38] A. I. Oliva, K. Gómez, G. González, and P. Ballester, "Diffusion-ordered spectroscopy (^{1}H-DOSY) of Zn-porphyrin assemblies induced by coordination with DABCO," *New J. Chem.*, vol. 32, no. 12, pp. 2159–2163, 2008, doi: 10.1039/b806932h.

[39] R. J. Klingler and J. K. Kochi, "Electron-transfer kinetics from cyclic voltammetry. Quantitative description of electrochemical reversibility," *J. Phys. Chem.*, vol. 85, no. 12, pp. 1731–1741, 1981, doi: 10.1021/j150612a028.

[40] D. T. Sawyer, G. Chlerlcato, C. T. Angells, E. J. Nanni, and T. Tsuchiya, "Effects of Media and Electrode Materials on the Electrochemical Reduction of Dioxygen," *Anal. Chem.*, vol. 54, no. 11, pp. 1720–1724, 1982, doi: 10.1021/ac00248a014.

[41] D. Vasudevan and H. Wendt, "Electroreduction of oxygen in aprotic media," *J. Electroanal. Chem.*, vol. 392, no. 1–2, pp. 69–74, 1995, doi: 10.1016/0022-0728(95)04044-O.

[42] P. Cofré and D. T. Sawyer, "Electrochemical Reduction of Dioxygen to Perhydroxyl ($HO_2^{\cdot}$) in Aprotic Solvents That Contain Brønsted Acids," *Anal. Chem.*, vol. 58, no. 6, pp. 1057–1062, 1986, doi: 10.1021/ac00297a017.

[43] A. Apffel, J. A. Chakel, S. Fischer, K. Lichtenwalter, and W. S. Hancock, "Analysis of oligonucleotides by HPLC-electrospray ionization mass spectrometry," *Anal. Chem.*, vol. 69, no. 7, pp. 1320–1325, 1997, doi: 10.1021/ac960916h.

[44] N. Gupta and H. Linschitz, "Hydrogen-bonding and protonation effects in electrochemistry of quinones in aprotic solvents," *J. Am. Chem. Soc.*, vol. 119, no. 27, pp. 6384–6391, 1997, doi: 10.1021/ja970028j.

[45] D. L. Maricle and W. G. Hodgson, "Reduction of Oxygen to Superoxide Anion in Aprotic Solvents," *Anal. Chem.*, vol. 37, no. 12, pp. 1562–1565, 1965, doi: 10.1021/ac60231a027.

[46] C. P. Andrieux, P. Hapiot, and J. michel Saveant, "Mechanism of Superoxide Ion Disproportionation in Aprotic Solvents," *J. Am. Chem. Soc.*, vol. 109, no. 12, pp. 3768–3775, 1987, doi: 10.1021/ja00246a040.

[47] R. H. Wopschall and I. Shain, "Effects of Adsorption of Electroactive Species in Stationary Electrode Polarography," *Anal. Chem.*, vol. 39, no. 13, pp. 1514–1527, 1967, doi: 10.1021/ac50156a018.

[48] P. Cofr and D. T. Sawyer, "redox chemistry of H_2O_2," *Inorg. Chem.*, no. 7, pp. 2089–2092, 1986.

[49] A. Berkessel, J. A. Adrio, and D.- Ko, "Dramatic Acceleration of Olefin Epoxidation in Fluorinated Alcohols : Activation of Hydrogen Peroxide by Multiple H-Bond Networks," no. 6, pp. 13412–13420, 2006.

[50] Y. Yi *et al.*, "Electrochemical corrosion of a glassy carbon electrode," *Catal. Today*, vol. 295, no. February, pp. 32–40, 2017, doi: 10.1016/j.cattod.2017.07.013.

[51] G. Laus, "Kinetics of acetonitrile-assisted oxidation of tertiary amines by hydrogen peroxide,"

J. Chem. Soc. Perkin Trans. 2, no. 6, pp. 864–868, 2001, doi: 10.1039/b102066h.

Supporting Information

Product workup and characterization

1-Phenylpentane-1,4-dione (7)

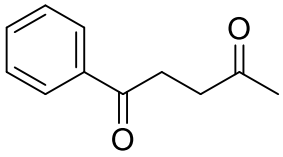

Into a reaction vessel 44 mg (0.4 mmol) of quinuclidine, 64 mg (0.4 mmol) of tetramethylammonium tetrafluoroborate, 65 mg (0.4 mmol) of valerophenone and 400 µL (4 mmol) of 1,1,1,3,3,3-hexafluoropropan-2-ol and 3.6 mL of acetonitrile were added. Reactants were dissolved by sonication of the solution. After sonication a glassy carbon anode, nickel foam cathode and a non-aqueous reference electrode were lowered in the solution. No considerations were given to exclude moisture or air. A current of 10 mA was then applied for 18 h.

After the reaction, the mixture was transferred to a 100 mL roundbottom flask and evaporated under reduced pressure. The residue was dissolved in EtOAc (50 mL), transferred to a separation funnel and washed with aq. sat. $NaHCO_3$ (20 mL) and brine (20 mL). The organic phase was separated, dried over anhydrous $MgSO_4$ and evaporated under reduced pressure. The residue was purified using automated flash chromatography (SiO_2, 12 g cartridge, 15 mL/min, 100 % heptane for 5 min to 90% heptane/10% EtOAc over 10 min followed by 90% heptane/10% EtOAc for 10 min). The *title compound* was obtained as a colorless oil (38 mg, 0.216 mmol, 54%). Additionally, unreacted valerophenone was recovered as a colorless oil (25 mg, 0.15 mmol, 38%).

Colorless oil, ^{1}H NMR (400 MHz, $CDCl_3$): δ 7.99-7.97 (m, 2H), 7.56 (t, J = 7.6 Hz, 1H), 7.46 (t, J = 7.7 Hz, 2H), 3.28 (t, J = 6.1 Hz, 2H), 2.89 (t, J = 6.1 Hz, 2H), 2.26 (s, 3H) ppm. ^{13}C NMR (101 MHz, $CDCl_3$): δ 207.4 (C), 198.6 (C), 136.8 (CH), 133.3 (CH), 128.7 (CH), 128.2 (CH), 37.2 (CH_2), 32.6 (CH_2), 30.2 (CH_3) ppm. LC-MS (ESI) for $C_{11}H_{13}O_2$ $[M+H]^+$ calcd. 177.0910, found 177.1.

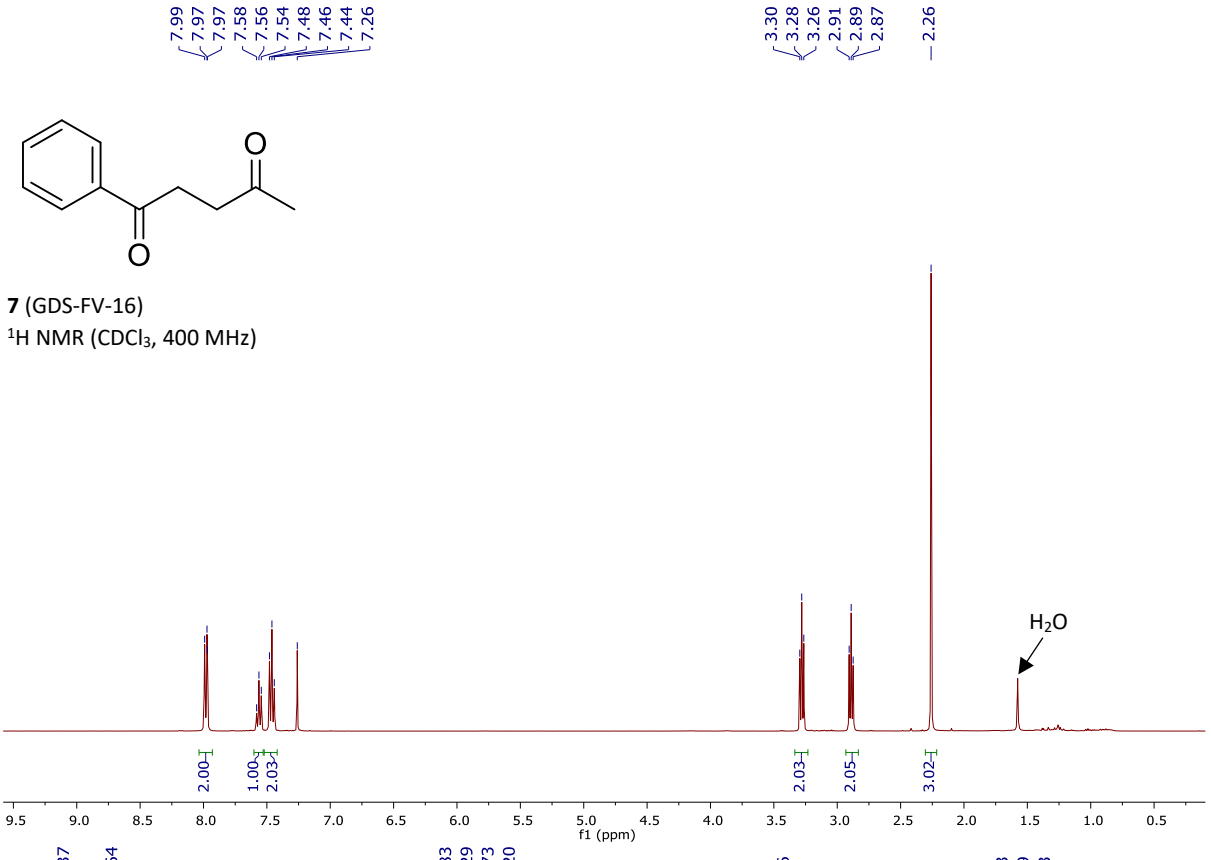

7 (GDS-FV-16)
^{1}H NMR ($CDCl_3$, 400 MHz)

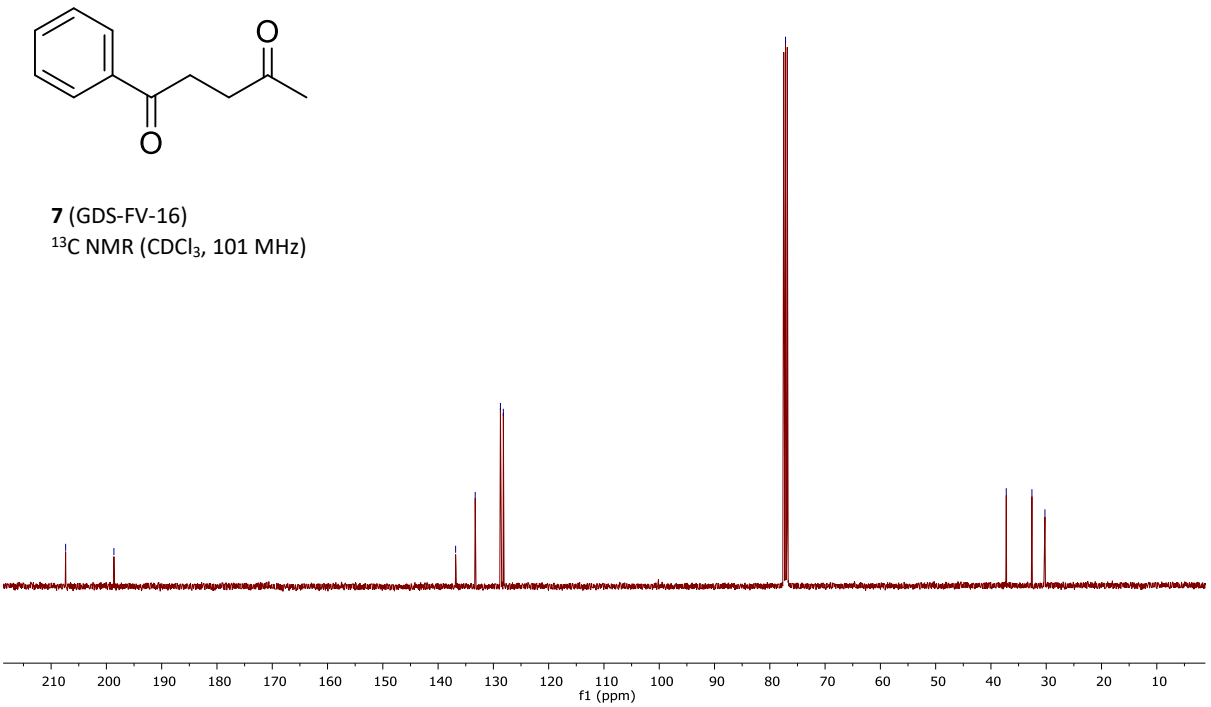

7 (GDS-FV-16)
^{13}C NMR ($CDCl_3$, 101 MHz)

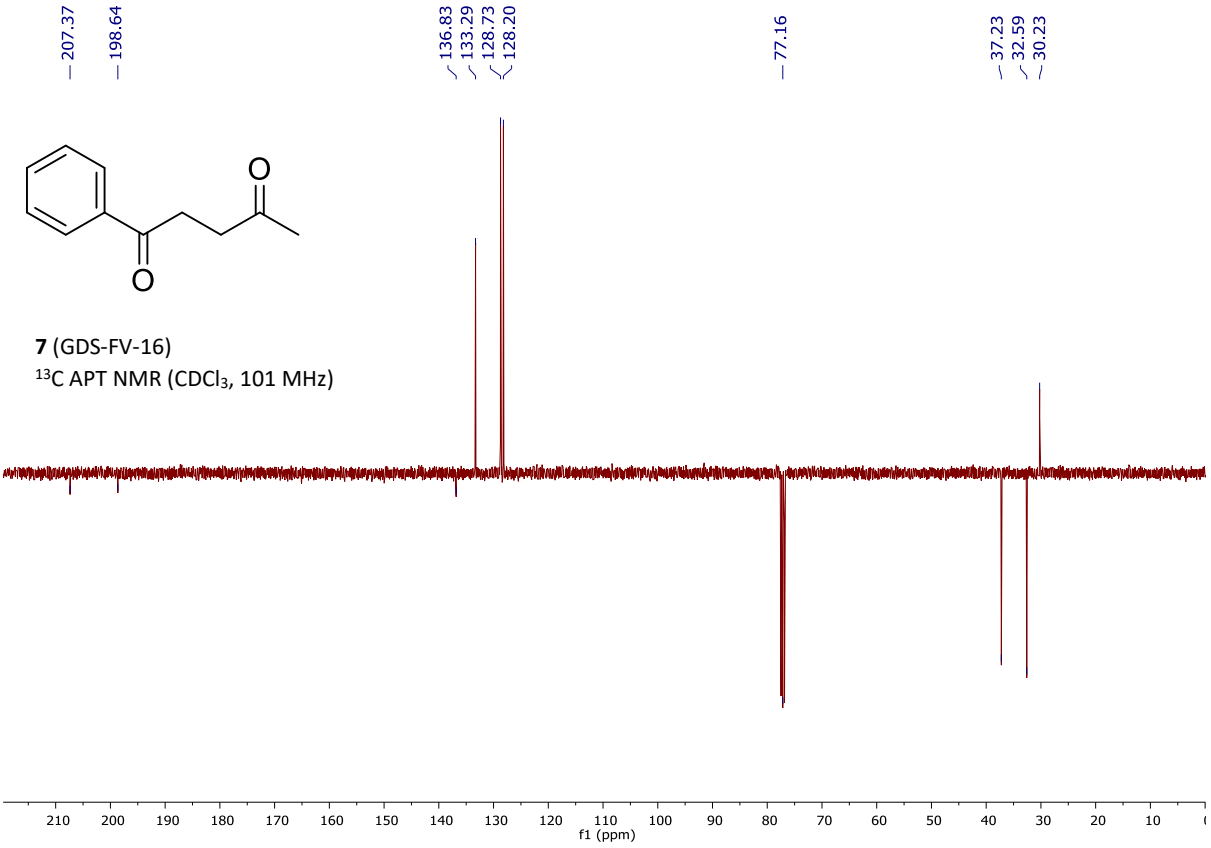

7 (GDS-FV-16)
^{13}C APT NMR ($CDCl_3$, 101 MHz)

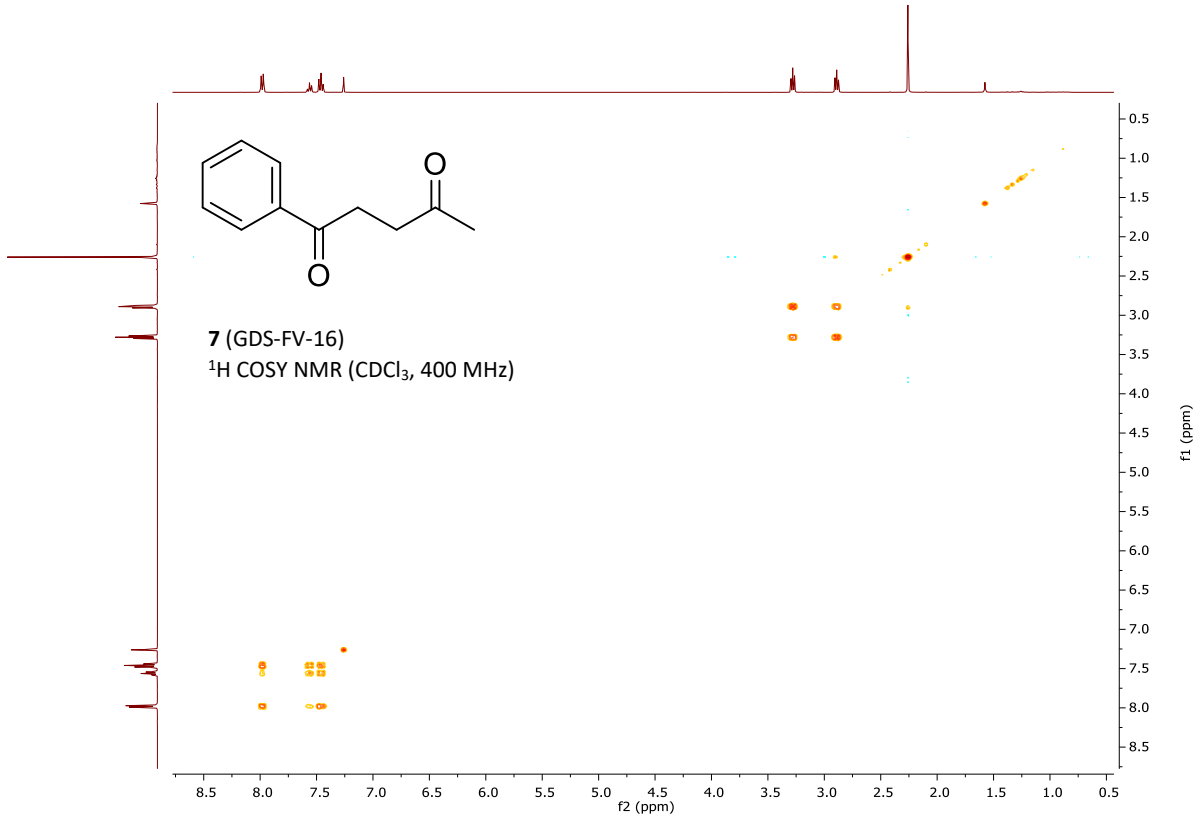

7 (GDS-FV-16)
^{1}H COSY NMR ($CDCl_3$, 400 MHz)

Synthesis procedure for quinuclidine N-Oxide

We have followed the synthesis procedure described by CAS (reaction number 31-506-CAS-20830963).

Add 100 mg (0.9 mmol, 1 equiv.) of quinuclidine to 1.8 mL of methanol in a sealed tube. Add 0.17 ml of 33% aqueous H_2O_2 (1.8 mmol, 2 equiv.) dropwise. Seal the tube and heat at 90 °C for 3 hours. Remove from heat and concentrate crude to obtain an oily residue. Purify the crude by filtration through basic alumina (1 g, 9:1 CH_2Cl_2:isopropanol) to afford quinuclidine N-oxide (96% yield).

3.5.2 Side Reactions

DFT analysis of the Lowdin charge densities of atoms on HFIP, HFIP anion and HFIP adduct have been performed using Orca software [1] with a PBE0 [2] hybrid functional, with a RIJCOSX [3] approximation, D3 dispersion correction [4] and BJ damping[5], def2-TZVP [6] basis set with an auxiliary def2-J[7] basis set. Structure optimizations have been carried out with a CPCM solvation model for acetonitrile. Geometry of all the molecules was optimized, followed by frequency optimization.

From table 1 it is possible to see that unbounded HFIP possesses the highest charge density on the H of the C-H bond, therefore it is this state which will most likely be activated by Qn.

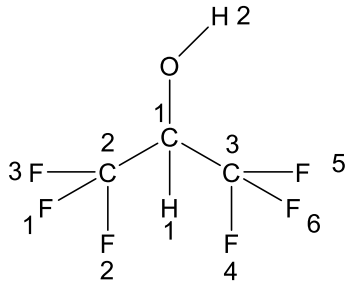

Figure 1

Labeling of the HFIP molecule

	Lowdin atomic charges		
	HFIP	HFIP anion	Qn-HFIP
H1	0.190539	0.140008	0.184928

Table 1

Loewdin atomic charges on C-H H1 atom

Presence of 1,1,1,3,3,3-hexafluoropropan-2-one (HFA) was confirmed by injecting a standard of HFA hydrate in ACN into the GCMS. In fig. 2A it's possible to see the chromatograms, in which the HFA product peak overlays with the standard. In fig. 2B the spectra of the standard and product can be seen. They overlay nearly perfectly, thereby confirming indeed the presence of HFA in solution.

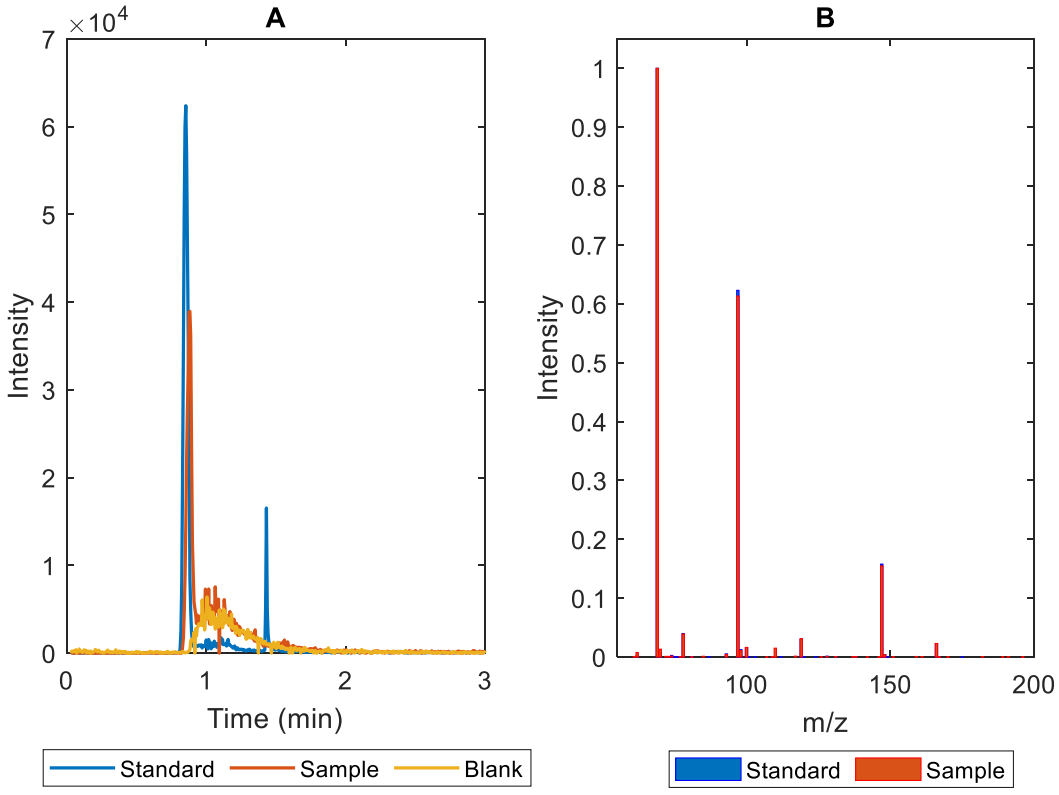

Figure 2

A) chromatograms of HFA and B) spectra of HFA

Bibliography

[1] F. Neese, "Orca software." https://orcaforum.kofo.mpg.de/app.php/portal.

[2] C. Adamo and V. Barone, "Toward reliable density functional methods without adjustable parameters: The PBE0 model," *J. Chem. Phys.*, vol. 110, no. 13, pp. 6158–6170, 1999, doi: 10.1063/1.478522.

[3] S. Kossmann and F. Neese, "Efficient structure optimization with second-order many-body perturbation theory: The RIJCOSX-MP2 method," *J. Chem. Theory Comput.*, vol. 6, no. 8, pp. 2325–2338, 2010, doi: 10.1021/ct100199k.

[4] S. Grimme, S. Ehrlich, and L. Goerigk, "Effect of the damping function in dispersion corrected density functional theory," *J. Comput. Chem.*, vol. 32, no. 7, pp. 1456–1465, 2011, doi: https://doi.org/10.1002/jcc.21759.

[5] A. D. Becke and E. R. Johnson, "Exchange-hole dipole moment and the dispersion interaction," *J. Chem. Phys.*, vol. 122, no. 15, 2005, doi: 10.1063/1.1884601.

[6] T. H. Dunning, "Gaussian basis sets for use in correlated molecular calculations. I. The atoms boron through neon and hydrogen," *J. Chem. Phys.*, vol. 90, no. 2, pp. 1007–1023, 1989, doi: 10.1063/1.456153.

[7] F. Weigend, "Accurate Coulomb-fitting basis sets for H to Rn," *Phys. Chem. Chem. Phys.*, vol. 8,

no. 9, pp. 1057–1065, 2006, doi: 10.1039/b515623h.

[8] “Avogadro advanced molecular editor.” https://avogadro.cc/.